

pubs.acs.org/cm Article

Co-Assembly of Functionally Active Proteorhodopsin Membrane Protein Molecules in Mesostructured Silica—Surfactant Films

Published as part of the Chemistry of Materials virtual special issue "In Honor of Prof. Clement Sanchez".

Maxwell W. Berkow, Hosu Gwak, Matthew N. Idso, Michael B. Schmithorst, Bailey E. Rhodes, Brad D. Price, Daniel S. Gianola, Songi Han, and Bradley F. Chmelka*



Cite This: Chem. Mater. 2023, 35, 8502-8516



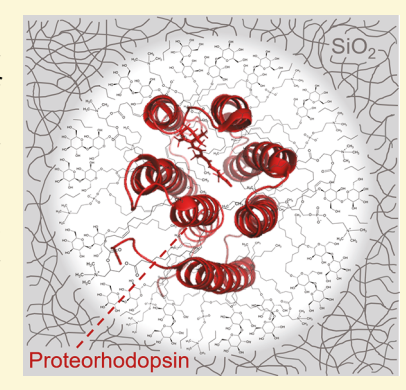
ACCESS

III Metrics & More

Article Recommendations

supporting Information

ABSTRACT: A combination of nonionic, cationic, and zwitterionic surfactants is shown both to stabilize the transmembrane protein proteorhodopsin, as well as to direct coassembly into robust transparent mesostructured silica—surfactant films containing high loadings of functionally active protein guests. Proteorhodopsin is a transmembrane protein that exhibits light-activated H $^+$ transport properties, the photocycle kinetics of which are quantified by time-resolved UV—visible spectroscopy and demonstrated to be similar to proteorhodopsin in the abiotic mesostructured films compared to native-like lipids. The surfactants mediate the pK_a of a key ion-channel residue, leading to an expanded pH functional range for proteorhodopsin in mesostructured silica—surfactant host materials. Small-angle X-ray diffraction results for $100-\mu m$ films show high extents of mesoscale order with protein loadings up to 25 wt % and wormlike mesostructural order for 44 wt % proteorhodopsin. Solid-state 1H , ^{13}C , and ^{29}Si NMR analyses provide atomic-scale insights into the compositions and interactions at the mesochannel surfaces, which account for the structure-directing roles of surfactant species. Nanoindentation measurements reveal the



mechanical robustness of the films, which interestingly increases with proteorhodopsin loading for the compositions examined. Heat treatment analyses show improved thermal stability for proteorhodopsin to 110 °C within mesostructurally ordered films. The results establish closely correlated relationships between the compositions, nano- and mesoscale structures, photocycle kinetics, and macroscopic mechanical properties and thermal stabilities of the silica—surfactant- proteorhodopsin films, providing key biomimetic design criteria.

■ INTRODUCTION

Membrane proteins perform within cellular environments a variety of transport, sensing, and catalytic functions that are attractive for technological applications. For example, the transmembrane protein proteorhodopsin transports H⁺ ions in response to light, thus converting solar energy into a chemical (pH) gradient. 1-3 Protein engineering strategies are improving the stabilities and enhancing and diversifying the properties of membrane proteins beyond their native functions.⁴ Protein guest molecules can be incorporated into non-native abiotic hosts, such as polymers, glasses, and mesostructured hybrid materials, with diverse macroscopic morphologies, including particles, fibers, films, or monoliths to improve the mechanical or thermal stabilities of the protein-host system. For example, globular proteins can be postsynthetically adsorbed onto the surface of porous materials through hydrogen bonding, electrostatic forces, or hydrophobic effects; however, these interactions are often transient or weak, and leaching of the protein can lead to a loss in activity. Alternatively, biologically enabled materials can be made through the coassembly and subsequent cross-linking of polymeric or inorganic oxide

matrices around protein moieties, producing uniform distributions of stable and functionally active guest molecules. Incorporation of functionally active protein during syntheses of many of these materials has been challenging, due in part to the often countervailing chemical compositions or conditions required to maintain protein stability compared with those typically used to synthesize or process polymeric or inorganic

As a host material for proteins, silica is a good candidate because it is mechanically and thermally robust and can be synthesized under relatively mild conditions. While many mesostructured silica materials have been synthesized under conditions that typically denature proteins, such as very high or low pH or with high concentrations of organic solvents,

Received: May 29, 2023 Revised: August 25, 2023 Published: October 5, 2023





extensive previous work has demonstrated that silica can be synthesized in aqueous sol—gel mixtures at pH values in the range of 5–8.8 These relatively benign conditions make sol—gel-derived materials suitable for protein incorporation, whereby hydrolyzed siloxane precursors cross-link around typically globular proteins that are occluded within robust inorganic host matrices. Such protein-silica materials are processable into monoliths or thin films, although typically with low protein loadings and often unfavorable or transient interactions between the protein guests and the silica matrix that alter protein function and reduce stability.

Compared to globular proteins, transmembrane proteins are particularly challenging to incorporate into non-native host environments due in part to their heterogeneous amphiphilic characters. While useful for relatively hydrophilic globular proteins, hydrophilic host environments such as silica are generally incompatible with the highly hydrophobic transmembrane regions of membrane proteins. Most transmembrane proteins are made up of hydrophobic α -helices that span the lipid bilayer of cell membranes, with hydrophilic loops that are exposed to aqueous environments at the intra- and extracellular sides of the bilayer. Such amphiphilicity can be exploited by using surfactants to simulate native-like cell membrane conditions in abiotic host environments, such as liposomes or micelles. ^{10–12} In fatty-acid—based lipid bilayers of liposomes, hydrophobic lipid chains stabilize the α -helices of the membrane protein, whereas the charged and hydrophilic lipid headgroups at the cytoplasmic and extracellular interfaces stabilize the protein. 13 However, these bilayers, native or synthetic, exhibit poor mechanical and thermal stabilities and are also not easily processable into macroscopic material morphologies. Amphiphilic block copolymers similarly provide both hydrophilic and hydrophobic regions that offer suitable synthetic environments to stabilize membrane proteins with better mechanical and chemical stabilities, as well as local orientational order. 14-16 These wholly organic-amphiphilebased synthetic hosts accommodate modest bulk amounts of membrane proteins, with still relatively poor mechanical properties. 14-16

For optically responsive molecules such as proteorhodopsin, it is additionally necessary for the host materials to be optically transparent. Previously, highly hydrophobic photoresponsive conjugated polymers have been incorporated into transparent surfactant-directed silica and titania matrices with significant extents of mesostructural order. Similar mesostructured materials have been used to accommodate other molecular guests, such as low-molecular-weight dyes and nanoparticles, although these hosts have generally been synthesized using nonaqueous solvents that are incompatible with proteins.

Here, we report novel transparent and robust silicasurfactant films with high extents of mesostructural order and that incorporate high loadings of functionally active transmembrane protein proteorhodopsin guests. This unusual combination of properties is enabled by the judicious selection of three types of surfactants and synthesis conditions, which both stabilize the membrane protein and direct its coassembly into the hydrophobic regions of the mesostructured silicasurfactant host materials, which can be processed into films up to 1 mm thick with arbitrary lateral dimensions. Small-angle X-ray scattering analyses elucidate the protein-stabilizing and structure-directing roles of the surfactants, while solid-state NMR resolves molecular-level interactions between the

surfactants and mesochannel silica surfaces. Notably, time-resolved UV—visible absorption spectra quantify the photocycle kinetics of the proteorhodopsin guests, which retain their native-like light-activated conformational dynamics within the mesostructured silica—surfactant materials, even at high protein loadings.

■ EXPERIMENTAL SECTION

Protein Expression and Purification. The monomer-enriched proteorhodopsin mutant E50Q (Figure 1a) was cloned into a pET26b

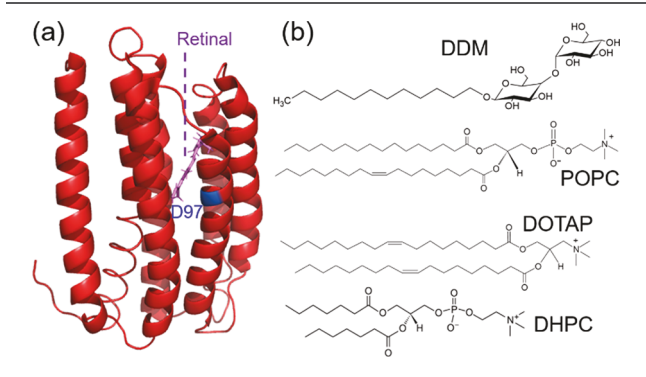


Figure 1. Schematic diagrams of (a) the E50Q mutant form of the transmembrane protein proteorhodopsin (PR) with 7 α-helices, lightresponsive retinal moiety, and key ion-channel aspartic acid residue D97; (b) nonionic C_{12} -maltoside n-dodecyl- β ,p-maltoside (DDM) surfactant, zwitterionic 1-palmitoyl-2-oleoyl-glycero-3-phosphocholine (POPC) lipid, cationic 1,2-dioleoyl-3-trimethylammonium-propane (DOTAP) lipid, and zwitterionic 1,2-diheptanoyl-sn-glycero-3-phosphocholine (DHPC) lipid.

(+) vector (Novagen) as described previously.²⁵ For expression, 10 mL cultures of BL21(DE3) E. coli (Thermo Fisher), transformed with the above plasmid, were made in LB broth with 50 $\mu g/mL$ kanamycin and orbitally shook at 180 rpm for 16 h at 37 °C. These cultures were diluted into 1 L of LB with 50 µg/mL kanamycin and grown at 37 °C with 180 rpm orbital shaking until $OD_{600} = 0.6$, at which point PR expression was induced with 1 mM isopropyl β_{D} -1-thiogalactopyranoside (IPTG, Thermo Fisher) and 1 μM trans-retinal (Sigma-Aldrich). Trans-retinal is essential for PR function, and the cells cannot produce it on their own. After 18 h, each liter of cell culture was spun down at 5000 rcf, resuspended in 30 mL of 50 mM K₂HPO₄ (Sigma-Aldrich) and 150 mM KCl (Sigma-Aldrich) (PR buffer) at pH 8.7, and then lysed for 1 h with incubation in lysis buffer (20 mg/mL lysozyme, DNase and 20 mM MgCl₂). Lysed cells were then centrifuged at 1000 rcf for 10 min to remove large debris in the pellet. The supernatant was then spun down at 10,000 rcf to harvest PRcontaining membranes in the new pellet. The supernatant was removed, and the membranes were flash frozen as pellets in liquid nitrogen and stored at -80 °C until needed for experiments. Purification of PR began with homogenization of the membrane pellet in 2 wt % n-dodecyl- β ,D-maltoside (DDM, Anatrace) PR buffer with a glass tissue grinder and then mixed for 1 h. The homogenized solution was spun down at 100,000 rcf and the supernatant collected to obtain PR E50Q in DDM micellar solution. Next, PR was further purified using a 5 mL Ni-NTA resin column (ThermoFisher) with a binding buffer (0.01 wt % DDM and 30 mM imidazole) and eluting buffer (0.01 wt % DDM and 500 mM imidazole). Prior to incorporation into materials, the ionic strength of the PR-containing solutions was lowered by using a PD-10 desalting column (Millipore) and then concentrating the eluate as desired by centrifugal concentration (50 kDa MWCO, Amicon Ultra), generally >100 μM. Protein concentration was determined using the absorbance at 520 nm using an extinction coefficient of 49,000 M⁻¹ cm and a molecular weight of 29,000 g/mol.

Preparation of Proteorhodopsin-Containing Silica-Surfactant Films. Mesostructured silica materials were prepared by mixing a 3:1 ratio by weight of 262.5 mg of tetraethoxysilane (TEOS, Acros Organics) and 87.5 mg of n-propyltriethoxysilane (PTEOS, 97%, Alfa Aesar) with 1.5 g of H_2O and 10 μL of 400 mM HCl. The solution was stirred vigorously for 3 h, at which point the solution was transparent. Two hundred milligrams of this solution were removed and mixed with an appropriate amount of DDM, n-decyl-β,Dmaltoside (DM, Anatrace), or n-hexadecyl- β ,D-maltoside (HDM, Anatrace). Another solution was created by mixing a desalted PRcontaining DDM micellar solution with a 9.1 wt % solution of 1palmitoyl-2-oleoyl-glycero-3-phosphocholine (POPC, Avanti Polar Lipids) and 1,2-dioleoyl-3-trimethylammonium-propane (DOTAP, Avanti Polar Lipids) in 4:1 molar ratio or, for comparative pK_a measurements, with 1,2-diheptanoyl-sn-glycero-3-phosphocholine (DHPC, Anatrace); the molecular structures are shown in Figure 1b. The two solutions were then mixed and quickly titrated to a pH of 4.1 using 50 mM HCl or 50 mM NaOH. The final concentration of species in this mixed solution depended on the desired PR loading; however, ratios of the other components were kept fixed at 62.5 maltoside surfactant: 6.1 POPC: 1.4 DOTAP: 22.5 SiO₂: 7.5 npropyl-SiO_{1.5} by weight. The amount of the maltoside surfactant added to the silica precursor solution (as discussed above) is dependent on the concentration of the maltoside surfactant in the protein-stabilizing micelles, measured via 1D solution-state ¹H NMR, which varies for different expressions. Final solutions were cast onto PDMS stamps (~2 cm × 2 cm) or Si wafers with a fluoro-monolayer (for mechanical property testing) under ambient temperature and 58% relative humidity conditions for films with rectangular or cubic mesostructural ordering and at 98% relative humidity for films with wormlike mesostructural order. Solvent evaporation was allowed to proceed for 4 days before the materials were characterized. Synthesized films had thicknesses >100 μ m. Films made with predominantly DM- and HDM-structure-directed surfactants still contained small concentrations of DDM, which was used in the expression and purification of PR.

Material Characterization. Small-angle X-ray scattering (SAXS) was used to assess the impact of synthesis conditions on the longrange mesostructural ordering of the silica-surfactant-proteorhodopsin films. SAXS records the pattern of a continuously scattered beam of X-rays incident on a sample. With knowledge of the distance between the sample and the detector, the angles of reflection of the Xray path due to interactions with the material can be calculated. Wellordered samples will cause the scattered X-rays to be concentrated at certain positions and angles, whereas disordered samples will scatter X-rays in all directions, leading to a broad distribution of X-rays across the detector. The positions and intensities of the SAXS reflections show high extents of mesostructural order that can be analyzed to calculate d-spacings that correspond to characteristic scattering distances, such as the mean center-to-center dimensions between surfactant-directed silica mesochannels. SAXS measurements were conducted on a custom instrument using a XENOCS Genix 50W Xray microsource with Cu K α radiation ($\lambda = 1.542$ Å, voltage 50 keV, current 1 mA), a focus size of 50 μ m, a XENOCS FOX2D multilayer optics for SAXS monochomator, and a Dectris EIGER R 1M detector $(77.2 \text{ mm} \times 79.9 \text{ mm} \text{ sensitive area, } 1030 \times 1065 \text{ 32 bit image})$ located 1.7 m behind the sample. SAXS patterns were recorded over a range of $1-2.7 \ q \ (nm^{-1})$.

A two-dimensional (2D) 29 Si{ 1 H} HETCOR NMR analysis of 5 wt % PR, 59.4 wt % DDM, 5.8 wt % POPC, 1.3 wt % DOTAP, 21.4 wt % SiO₂, and 7.1 wt % n -propyl-SiO_{1.5} was performed at 11.7 T on a Bruker Avance NMR spectrometer equipped with a double-resonance 4 mm NMR probehead operating at frequencies of 500.2 MHz for 1 H and 99.4 MHz for 29 Si. 26 The experiment was performed at a magicangle-spinning frequency of 12.5 kHz and room temperature. For the experiment, 48 increments of 512 scans with an t_1 increment of 96 μ s were acquired. The recycle delay between scans was set to 1.2 s to correspond to 1.4 t_1 , where the 1 H t_1 was measured by a saturation recovery experiment. A 50 kHz 90° radiofrequency (r.f.) pulse was used for the initial excitation of 1 H nuclei, and a 1 ms cross-

polarization contact pulse was used to transfer polarization from ¹H to ²⁹Si nuclei. The ¹H and ²⁹Si contact pulse frequencies were optimized to maximize 29 Si signal intensity. During the t_1 evolution period, eDUMBO-122 homonuclear decoupling was applied to the 1H channel to enhance the resolution of the ¹H dimension.²⁷ SPINAL-64 heteronuclear decoupling was applied to ¹H nuclei during acquisition. ²⁸ Solution-state 2D ¹H–¹³C HSQC NMR spectra of POPC and DOTAP were acquired at 300 K on a Bruker Avance NMR spectrometer at a field of 18.8 T equipped with a 5 mm PABBO BB ¹H/D Z-GRD probehead operating at frequencies of 800.2 MHz for ¹H and 201.2 MHz for ¹³C (Figures S1 and S2). The highresolution solution-state 2D ¹H-¹³C NMR spectra were used to assign the ¹H signals in the solid-state 2D ²⁹Si{¹H} HETCOR NMR analysis. The 2D spectra were acquired using a phase-sensitive gradient HSQC experiment with echo/anti-echo detection (hsqcetgp pulse program in the Bruker library) with 256 increments of 16 scans and a recycle delay of 1.5 s between scans. The ¹³C and ¹H spectral widths were 166 and 13 ppm centered at 94 and 6 ppm, respectively. GARP decoupling was used to decouple ¹³C from detected ¹H spins during acquisition. A 2-fold linear forward prediction with 32 linear prediction coefficients was applied to the indirect dimension when processing the data. The samples were prepared as follows: stock solutions of POPC and DOTAP in chloroform (25 mg/mL) were blow-dried under a stream of N2 gas and further dried under vacuum overnight to remove residual chloroform. Then, samples were redissolved in CDCl₃ to final concentrations of 33 mM for NMR experiments. Solution-state 2D 1H-13C HSQC NMR spectra of DDM in D₂O were acquired at 300 K on a Varian VNMRS NMR spectrometer at a field of 14.1 T, equipped with a 5 mm AutoXDB PFG probehead operating at frequencies of 599.7 MHz for ¹H and 150.8 MHz for ¹³C (Figure S3). Specifically, the 2D spectra were acquired using a gHSQCAD pulse program in the Varian library with 256 increments of 16 scans and a recycle delay of 1.5 s between scans. The ¹³C and ¹H spectral widths were 220 and 16 ppm centered at 90 and 6 ppm, respectively. The ²⁹Si and ¹H NMR spectra were referenced indirectly to tetramethylsilane (TMS) at 0 ppm using tetrakis(trimethylsilyl)silane (TKS) as a secondary standard (-9.84 ppm for ²⁹Si, 0.25 ppm for ¹H).

Static visible absorption spectroscopy measurements were conducted on a Shimadzu UV-1800 spectrophotometer. For measurement of the pKa of D97, free-standing films of mesostructured silica were inserted into a home-built sample holder that fit into a transparent plastic cuvette. The sample was incubated initially in a solution containing 50 mM K_2HPO_4 and 150 mM KCl (pH ~ 8.7) for 15 min before UV-vis absorbance measurements were taken. Subsequently, the solution in the cuvette was removed and replaced with 2 mL of new buffered solution that had been titrated to the desired pH, one minute was allowed for incubation, the pH of the solution was measured, and the UV-visible absorbance of the film was taken. To determine the amount of time required for soaked films to equilibrate with the buffered solution, we monitored the visible absorbance of PR in the mesostructured silica after exposure to different buffered solutions; these measurements indicated that soaking as-synthesized films for 15 min and following this initial soak incubation times of 1 min in a new buffer were sufficient to allow equilibrium among PR species in the synthetic host and the buffered solution. Using an initial incubation time of 15 min and with 1 min of exposure to a new buffered solution between pH changes, this process was repeated using at least 11 buffered solutions that were at different pH values.

The absorbance data acquired from films soaked in different buffered solutions were analyzed by using a home-written MATLAB script to yield the acid dissociation constant for residue D97 of proteorhodopsin. The program calibrated each spectrum such that the absorbance intensity at 700 nm was zero and then normalized each absorption spectrum such that the absorbance maximum between 500 and 550 nm had an absorbance intensity of unity. Subsequently, the wavelength of maximum absorbance intensity was extracted and plotted as a function of pH. The resulting data were then fit to the

Henderson–Hasselbalch equation using a nonlinear fitting algorithm with two fitting constants, the pK_a value and the Hill coefficient.

Static UV—visible light absorbance measurements at 520 nm were conducted on 5 wt % PR-containing films before and after heat treatment for 24 h at various temperatures to determine the effect of the host matrix on the stability of guest proteorhodopsin. Films with rectangular mesostructural ordering were subjected to heat treatment at 70, 80, 90, 100, 110, 120, 130, 140, and 150 °C. Films with wormlike mesostructural ordering were tested up to 120 °C, at which point all of the guest PR molecules had been denatured. All measurements were taken through the center of each film, as aligned visually. The experimental uncertainties in these analyses are 5–10%, due in part to heterogeneity in the thickness of the sample and limitations of the sample alignment.

Transient UV-visible absorption data were acquired using a SpectraPro-500 Triple Grating Monochromator (Acton Research Corporation). Mesostructured silica films that incorporate proteorhodopsin were placed into borosilicate capillaries and measured either as-synthesized or after hydration at pH 9 in PR buffer for 1 week. During measurements, samples were illuminated using a whitelight-emitting halogen lamp; the transient response of proteorhodopsin, as well as the monochromator, was triggered using a SpectraPhysics Quanta-Ray Nd:YAG GCR-150 series 532 nm laser (pulse length \sim 5 ns, pulse power \sim 10 mJ). The absorbance intensities at 400, 410, 500, 510, 540, 570, 590, 620, and 630 nm were recorded over time scales ranging from 1 µs to 0.45 s (Figure S4). The absorption data at each wavelength were compiled together from 512 scans in which 500,000 absorbance data were measured over a linear time scale. The absorbance data at each wavelength were averaged over 200 equally spaced bins on a logarithmic scale and truncated at short times to remove artifacts from the laser. Global fitting analyses were performed with a home-build MATLAB code first reported by Idso et al.²⁹ These analyses were performed with two to seven exponential terms, and the sum of squared residuals decreased with each added term. However, global fit analyses performed with greater than three exponential terms for as-synthesized films in pH 4.1 environments or greater than five exponential terms for films hydrated to pH 9 showed significantly diminished improvements as well as the introduction of time constant values that were either repeated or outside the time range of collected data. These artifacts of the analyses indicate that the data for monomeric proteorhodopsin in DDM + POPC + DOTAP-structure-directed films are the best fit with five exponential time constants.

Nanoindentation measurements were performed to provide a rapid assessment of the indentation hardness and elastic modulus of mesostructured silica membranes as a function of their concentration of PR and silica. The films were cast on the fluorinated surface of a Si wafer to diminish adhesion to the substrate and thereby prevent strains as the mesostructured PR-silica—surfactant films formed. Small diameter films were used to minimize their surface curvatures, enabling an accurate determination of the tip area function and consistency in mechanical measurements between specimens. Nanoindentation measurements were performed using a Nanomechanics iMicro Nanoindenter equipped with a 1 N load cell and diamond Berkovich tip indenter, using load control at a constant strain rate of $0.2 \, \mathrm{s}^{-1}$, defined as $\frac{P}{r}$. All data were collected using a continuous

 0.2 s^{-1} , defined as $\frac{P}{p}$. All data were collected using a continuous stiffness method, where dynamic periodic oscillations were superimposed on the loading profile at a frequency of 100 Hz and an amplitude of 2.0 nm to enable the continuous measurement of properties as a function of the depth of the indent. In these experiments, indentations were performed to a maximum depth of 1 μ m and with a spacing of 20 μ m between neighboring indents to avoid overlap of plastic zones. Each measurement of hardness and modulus reported herein reflects the average (and standard deviation) of between 10 and 20 indents, quantified at depths between 300 and 1000 nm to exclude the effects of surface roughness. Measurements of force, indent depth, and contact stiffness were converted to elastic modulus using the Oliver and Pharr method. Nanoindentation measurements enable the direct determination of the reduced elastic

modulus $E_{\rm r}$ of the film, which was used to calculate the elastic modulus, $E_{\rm r}$ of the film using $\frac{1}{E_{\rm r}}=\frac{1-v^2}{E}$ and an estimated Poisson's ratio, $v_{\rm r}$ of 0.2.³¹

■ RESULTS AND DISCUSSION

Syntheses of Proteorhodopsin-Silica-Surfactant **Films.** The coassembly of functional membrane proteins into mesostructured silica films is a transient multicomponent process that requires judicious selection of synthesis compositions and conditions to achieve high degrees of mesostructural order and retention of proteorhodopsin function. Key design objectives are to incorporate high loadings of functionally active membrane proteins into robust abiotic host matrices that are processable into films with macroscopically uniform properties. Achieving these objectives simultaneously is challenging and requires trade-offs between countervailing synthesis considerations that often promote either protein stability or the formation of a mechanically stable host matrix but not both. We hypothesized that membrane-protein-stabilizing and structure-directing amphiphilic surfactants could be used to incorporate high loadings of functionally active guest proteins into mesostructurally wellordered silica-surfactant host matrices that also impart strong mechanical properties onto the host film. Syntheses of these materials are governed by (i) the thermodynamics of coassembly and interactions between the protein, surfactant, solvent, and silica species and (ii) the kinetic processes associated with the rates of solvent evaporation, coassembly of the component species, and polymerization of the silica into a robust cross-linked matrix. A slow rate of solvent evaporation is typically desirable to promote the coassembly of proteinsilica-surfactant films with high extents of mesostructural order before the silica polymerizes into a rigid matrix. Key factors that influence these processes and thus the properties of the film include pH, solvent, humidity, types and relative concentrations of surfactant species, silica precursors, and protein guest molecules. Screening across these conditions leads to an optimized combination of surfactants and hydrolyzed silica precursors in aqueous solution that enables the formation of robust, crack-free, and free-standing mesostructured films with high loadings of the functionally active membrane protein proteorhodopsin.

Many syntheses of mesostructured silica-surfactant materials have relied on extremes of acidic or alkaline conditions, e.g., pH > 10 or pH < 2, to slow the rate of silica polymerization. For highly alkaline conditions greater than pH 10, strong electrostatic interactions between cationic surfactant moieties and hydrolyzed silica anions promote their coassembly into well-ordered hybrid materials.³² By comparison, for highly acidic conditions below pH 2 (the isoelectric point of silica), hydrogen-bonding interactions between hydrophilic moieties of nonionic surfactants with hydrolyzed silica cations similarly lead to well-ordered hybrid materials.³³ Such conditions, however, are incompatible with many proteins and result in their denaturation. In particular, native proteorhodopsin has evolved in marine environments to function at pH \sim 8.2, although it retains its general structure and behavior over a broad range of pH 4–10.34,35 It can irreversibly denature at pH conditions outside of this range, due in part to ionization of protein side chains or backbone moieties. These trade-offs are summarized in Figure 2a. Nevertheless, robust, well-ordered, and homogeneous films can be synthesized at pH 4.1,

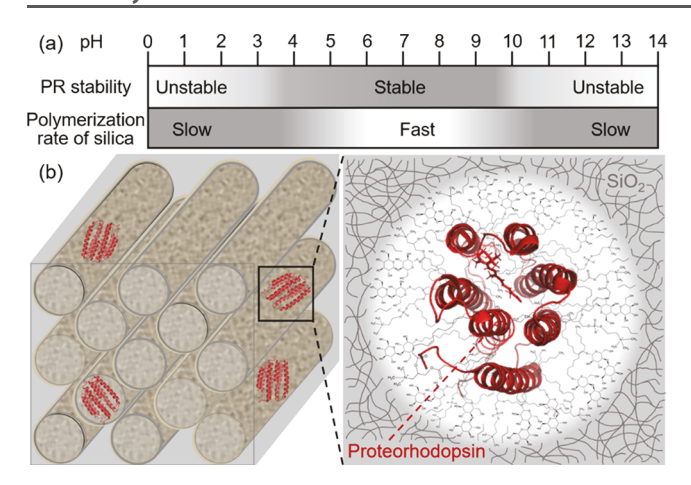


Figure 2. (a) Approximate pH ranges over which proteorhodopsin (PR) is stable in solution and corresponding relative ranges of silica polymerization rates.^{34–36} (b) Schematic diagram of a rectangular array of mesostructured silica—surfactant channels containing proteorhodopsin guests (red) and an enlarged region of a single proteorhodopsin molecule in a silica—surfactant mesochannel.

balancing the pH-dependent synthesis near the acidic limit of proteorhodopsin stability where comparatively slower silica polymerization rates can be achieved (Figure S5).³⁶

Coassembly of proteorhodopsin into mesostructured silicasurfactant host materials thus requires that the composition of the synthesis mixture be carefully balanced with respect to solvents, acidity, amphiphilicity, and ionicity of the surfactants, and silica precursor species. With respect to hydrolyzed, network-forming silica precursors, organosiloxane species have been shown to increase the hydrophobicity of the mesochannel surfaces, and at moderate concentrations yield surfactanttemplated silica materials with high extents of mesostructural order.^{37,38} Here, tetraethoxysilane (TEOS) was combined with *n*-propyltriethoxysilane (PTEOS) in a 3:1 ratio by weight, with the hydrophobic propyl moieties promoting interactions with the hydrophobic moieties of the structure-directing surfactants. Organic cosolvents, including ethanol produced by the hydrolysis of TEOS and PTEOS silica precursors, aid hydrolysis by solubilizing water-insoluble alkoxide precursors,³⁹ although they tend to denature proteorhodopsin in the presence of moderate concentrations of organic cosolvents. 40 Aqueous solutions also present challenges due to the highly hydrophobic transmembrane regions of membrane proteins, which require stabilizing surfactants to promote their solubility in solution. The judicious selection of surfactants with specific hydrophobic, hydrophilic, or charged moieties is also important for the incorporation of proteorhodopsin in silica-surfactant films. For example, the length of hydrophobic alkyl chains and the type and size of hydrophilic headgroups of surfactant species have been shown to increase both the stability of functionally active membrane proteins in aqueous solutions and promote greater extents of mesostructural order in silica. 40 Charged surfactant headgroups are also used to promote mesostructural order by increasing interactions between the surfactant and inorganic species. 41 However, charged headgroups can also lead to protein denaturation, necessitating careful selection of structure-directing surfactants for syntheses of mesostructured silica-surfactant host materials with functionally active proteorhodopsin. Conversely, neutral surfactants, both nonionic and zwitterionic, are often used to stabilize membrane proteins in micellar solutions and

rarely destabilize the protein. We hypothesized that favorable structure-directing features of the surfactants, such as relatively long alkyl chains and hydrophilic nonionic or charged headgroups, could be selected from amphiphilic surfactants known to stabilize membrane proteins and thereby used to incorporate high loadings of proteorhodopsin into a robust silica—surfactant film, as depicted in Figure 2b. Optimized synthesis conditions promote the formation of well-ordered mesostructured silica—surfactant host materials with significantly greater loadings of proteorhodopsin and mechanical robustness than previously reported. §

Surfactant and Protein Influences on the Mesoscale Order. A mixture of neutral and charged surfactants was identified to stabilize proteorhodopsin and direct its assembly into silica-surfactant host materials with high extents of mesostructural order. Nonionic alkyl-saccharide surfactants, specifically alkyl-glucosides and alkyl-maltosides, were identified as promising candidates because of their extensively studied protein-stabilizing properties in solution⁴⁰ and their separate propensity to direct the structures (without protein) of crack-free mesoporous films. 42 Alkyl-saccharide surfactants with varied chain lengths enable the dimensions of the mesochannel diameters to be adjusted to a characteristic length that is conducive for the incorporation of monomeric proteorhodopsin (PR, \sim 4 nm in length $\times \sim$ 3 nm in diameter). The lipids 1-palmitoyl-2-oleoyl-glycero-3-phosphocholine (POPC) and 1,2-dioleoyl-3-trimethylammonium-propane (DOTAP) were selected as cosurfactants to have a combination of protein-stabilizing and structure-directing properties. Specifically, a 4:1 molar ratio of POPC and DOTAP forms liposomes that stabilize PR and also favorably lowers the apparent pK_a of the key function-dependent D97 residue in proteorhodopsin,⁴³ enabling native-like photoactivation of PR at neutral pH. Individually, POPC is a zwitterionic lipid with a phosphocholine headgroup, which has been found to enrich the monomeric fraction of proteorhodopsin by disrupting protein-protein interactions. By comparison, DOTAP is a cationic surfactant that contributes to the lower pK_{aD97} and favorably promotes interactions with the anionic silica precursors. In addition, POPC and DOTAP each have two relatively long hydrophobic carbon chains that can be expected to promote a high extent of mesostructural

The ratio of the protein-stabilizing and structure-directing surfactant species to silica was selected to produce mesostructural order, either hexagonal or rectangular, based on the binary phase diagrams of these or similar surfactants in water. Furthermore, as water evaporates during synthesis, mesostructural order develops, according to precepts that have previously been reported. 44,45 The binary phase diagram of proteinstabilizing n-octyl- β -D-glucoside (OG) reveals a small synthesis space for the formation of a cylindrical hexagonal mesophase below 22 °C for 60-70 wt % OG and preferentially forming cubic or lamellar mesophases at higher temperatures or higher concentrations of surfactant. 46 In contrast, the binary phase diagram of n-dodecyl- β -D-maltoside (DDM) in water reveals that hexagonal or rectangular mesophases are favored at 20 °C over the range 45-80 wt % DDM, above which a multiphase mixture, including crystallized surfactant, results. 47 Thus, the larger disaccharide headgroup of DDM is expected to be preferred over glucoside surfactants for forming mesostructured PR-containing silica-surfactant materials. The composition of nonprotein molecules in PR-containing mesostruc-

tured silica—surfactant films was selected to be 70 wt % surfactant and 30 wt % silica, in the center of the hexagonal/rectangular synthesis space of the DDM-water binary phase diagram. The ratios of surfactants were further refined to balance the structure-directing and protein-stabilizing properties of DDM, POPC, and DOTAP, in particular, to overcome the poor solubility of the lipids in aqueous solutions. The optimized composition of nonprotein components in the mesostructured PR—silica—surfactant films investigated here was determined to be 62.5 wt % DDM, 7.5 wt % POPC/DOTAP (80/20, mol/mol), and 22.5 wt % SiO₂, and 7.5 wt % *n*-propyl-SiO_{1.5}. This balances the chain lengths, charges, and solubilities of surfactants with the anionic silica precursors in aqueous solution at pH 4.1 to produce a well-ordered mesostructured PR—host film.

The structure-directing properties of different alkyl-chain-length maltoside surfactants were optimized experimentally. Small-angle X-ray scattering (SAXS) was used to probe the mesostructural ordering of 5 wt % PR-containing silica—surfactant films synthesized under identical conditions, except for the use of maltoside surfactants with different hydrophobic alkyl chain lengths: n-decyl- β ,D-maltoside (C₁₀-maltoside, DM), n-dodecyl- β ,D-maltoside maltoside (C₁₂-maltoside, DDM), and n-hexadecyl- β ,D-maltoside (C₁₆-maltoside, HDM) (Figure 3). For example, 5 wt % PR-containing

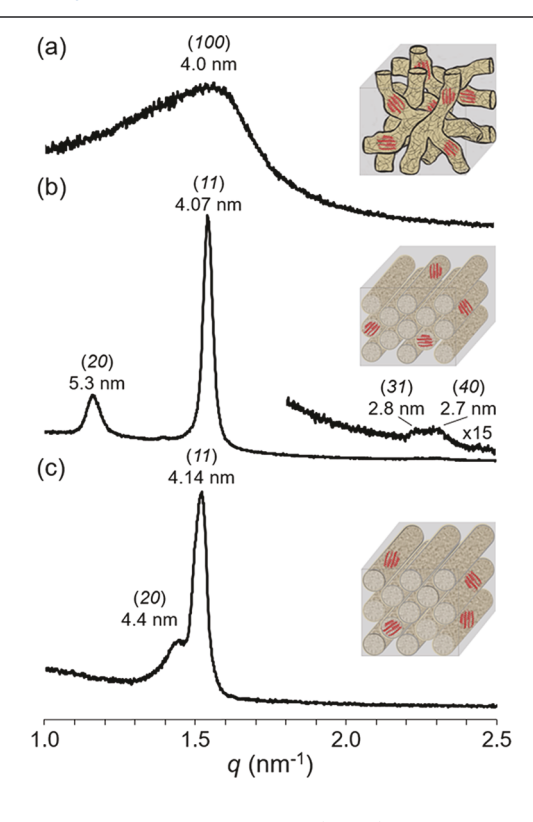


Figure 3. Small-angle X-ray scattering (SAXS) patterns for 200- μ m-thick mesostructured PR-surfactant-silica films synthesized using structure-directing maltoside surfactants with different alkyl chain lengths and overall compositions of 5.0 wt % PR, 5.8 wt % POPC, 1.3 wt % DOTAP, 21.4 wt % SiO₂, 7.1 wt % n-propyl-SiO_{1.5}, 9.5 wt % DDM from the expression and purification of PR, and 49.9 wt % additional structure-directing maltoside: (a) decylmaltoside (C_{10} -alkyl chain), (b) dodecylmaltoside (C_{12} -alkyl chain), and (c) hexadecylmaltoside (C_{16} -alkyl chain) surfactants. Each SAXS pattern is accompanied by a schematic diagram showing PR monomers (red) dispersed within mesostructured surfactant channels in silica (gray).

silica-surfactant films synthesized with 5.8 wt % POPC, 1.3 wt % DOTAP, 21.4 wt % SiO₂, 7.1 wt % *n*-propyl-SiO_{1.5}, 9.5 wt % DDM, and 49.9 wt % of the structure-directing C₁₀maltoside DM yield a single broad SAXS reflection at 1.57 nm^{-1} (Figure 3a), corresponding to a d-spacing of 4.0 nm that is characteristic of wormlike mesostructural ordering. By comparison, the SAXS pattern in Figure 3b acquired for a film containing 5 wt % PR synthesized under identical conditions except with the C₁₂-maltoside DDM shows two intense, narrow, and well-resolved reflections at 1.18 and 1.542 nm⁻¹, as well as weak higher-order reflections at 2.23 and 2.31 nm⁻¹. These are indexable as the (20), (11), (31), and (40) reflections of a rectangular mesophase with d-spacings of 5.3, 4.07, 2.8, and 2.7 nm, respectively, which manifest a high extent of mesostructural ordering that is corroborated by electron microscopy images in Figure S6 of the Supporting Information. For a 5 wt % PR-silica-surfactant film synthesized with a longer C₁₆-maltoside HDM surfactant, the SAXS pattern in Figure 3c exhibits a similar (11) reflection at 1.518 nm⁻¹, corresponding to a *d*-spacing of 4.14 nm, and a partially resolved (20) reflection at 1.43 nm⁻¹ (4.4 nm dspacing). These are also consistent with rectangular mesostructural order and a modestly larger center-to-center distance separating the larger cylindrical C₁₆-maltoside surfactant aggregates. The differences in the lengths of the alkyl chains of the C₁₀-, C₁₂-, and C₁₆-maltoside surfactants thus lead to significant differences in mesostructural order of the PRsilica-surfactant films, manifesting the importance of hydrophobic chain length on the coassembly and structures of these materials. As the C₁₂-maltoside surfactant DDM led to the highest extent of rectangular mesostructural order, it was used to synthesize all of the PR-containing silica-surfactant films investigated here, unless otherwise specified.

The incorporation of proteorhodopsin guest molecules into the hydrophobic mesochannels of PR-silica-surfactant films serves to swell their local dimensions, with the overall effect on mesostructural order depending on protein loading. For example, Figure 4 shows SAXS patterns acquired for mesostructured silica-surfactant films containing 0, 5, 15, 25, and 44 wt % proteorhodopsin, which were synthesized with the same 62.5 DDM (C₁₂-maltoside): 6.1 POPC: 1.4 DOTAP: 22.5 SiO₂: 7.5 *n*-propyl-SiO_{1.5} mass ratios by weight of nonbiological components under otherwise identical conditions. Each film exhibited a high degree of transparency and macroscopically uniform distributions of PR across the 1 cm diameter films. Nevertheless, significant differences are observed in the SAXS patterns of the respective films. For example, for mesostructured silica-surfactant films without PR, Figure 4a shows three resolved reflections at 1.30, 1.44, and 1.60 nm⁻¹ (full-width-half-maximum, fwhm, values of 0.035, 0.049, and 0.032 nm⁻¹, respectively), with d-spacings of 4.8, 4.4, and 3.9 nm, that are indexed to the (200), (210), and (211) planes of a Pm3n cubic mesophase. Interestingly, the inclusion of 5 wt % PR results in a silica-surfactant material with a well-ordered rectangular mesophase structure, as evidenced by narrow (20) and (11) reflections at 1.18 and 1.542 nm⁻¹ (0.049 and 0.036 nm⁻¹ fwhm, respectively) and also higher-order (31) and (40) Bragg reflections at 2.23 and 2.31 nm^{-1} , corresponding to d-spacings of 5.3, 4.07, 2.8, and 2.7 nm, respectively (Figures 3b and 4b). The displacements of the (20) and (11) reflections to higher d-spacings are consistent with PR swelling the hydrophobic regions of the mesostructured silica-surfactant films. The effect of increased

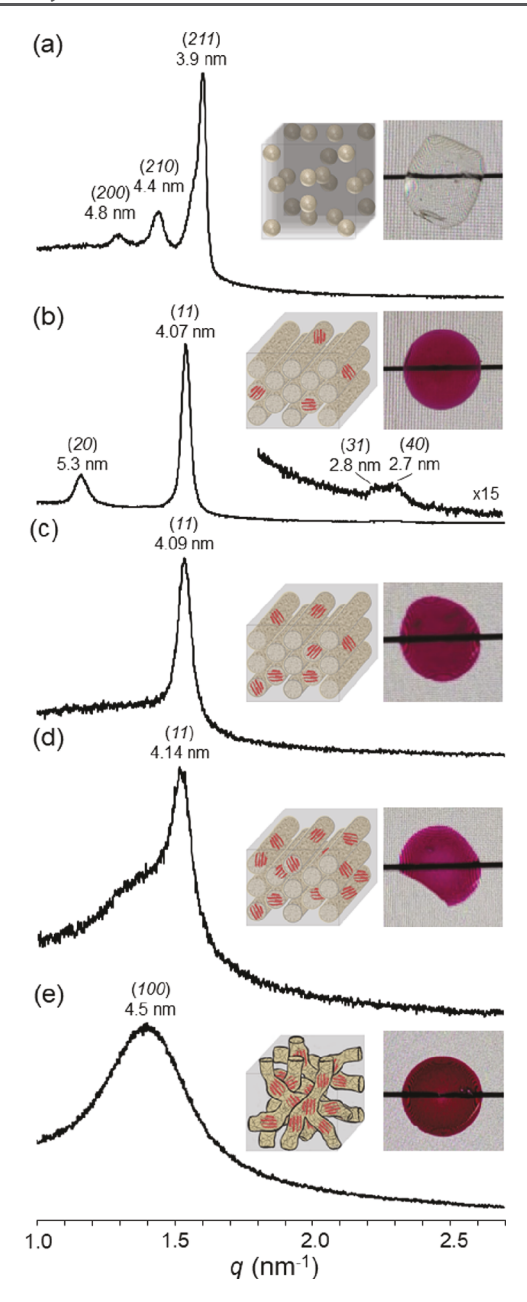


Figure 4. SAXS reflections of 200-µm-thick mesostructured proteorhodopsin (PR)-surfactant-silica films containing different protein loadings: (a) 0 wt % PR, 62.5 wt % DDM, 6.1 wt % POPC, 1.4 wt % DOTAP, 22.5 wt % SiO₂, 7.5 wt % n-propyl SiO_{1.5}, (b) 5 wt % PR, 59.4 wt % DDM, 5.8 wt % POPC, 1.3 wt % DOTAP, 21.4 wt % SiO₂, 7.1 wt % n-propyl SiO_{1.5}, (c) 15 wt % PR, 53.1 wt % DDM, 5.2 wt % POPC, 1.2 wt % DOTAP, 19.1 wt % SiO₂, 6.4 wt % n-propyl SiO_{1.5}, (d) 25 wt % PR, 46.9 wt % DDM, 4.6 wt % POPC, 1.0 wt % DOTAP, 16.9 wt % SiO₂, 5.6 wt % n-propyl SiO_{1.5}, and (e) 44 wt % PR, 35.0 wt % DDM, 3.4 wt % POPC, 0.8 wt % DOTAP, 12.6 wt % SiO₂, 4.2 wt % n-propyl SiO_{1.5}. Each SAXS pattern is accompanied by an optical image of the film and a schematic diagram showing PR monomers (red) dispersed within the mesostructured surfactant channels in silica (gray).

protein loading is observed in the SAXS pattern of a 15 wt % PR-silica—surfactant film shown in Figure 4c, for which a single narrow reflection is observed at $1.536~\rm nm^{-1}~(0.052~\rm nm^{-1}~fwhm)$, corresponding to a d-spacing of 4.09 nm, similar to but slightly broader than the (11) reflection of the 5 wt % PR-containing film. This reflection is also observed at $1.518~\rm nm^{-1}$

(4.14 nm d-spacing, Figure 4d) for a film with 25 wt % PR, which additionally yields another broader overlapping reflection centered at 1.33 nm⁻¹ (4.7 nm d-spacing). The relatively narrow (11) displaced reflections observed for 15 and 25 wt % PR-containing silica-surfactant films suggest moderate degrees of rectangular mesostructural ordering at these high protein loadings, although the absence of resolvable higher-order Bragg reflections prevents indexing to a specific phase. The broad reflection observed at 1.33 nm⁻¹ is consistent with increased swelling of the silica-surfactant mesochannels and the presence of worm-like mesostructural order. PRcontaining silica-surfactant films have been synthesized with up to 44 wt % functionally active PR, yielding a single broad SAXS reflection at 1.39 nm⁻¹ (Figure 4e), corresponding to a d-spacing of 4.5 nm, with the absence of higher order Bragg reflections indicative of worm-like mesostructural order. The worm-like mesostructural order exhibited by this film is due in part to the relatively low concentration of structure-directing surfactants (39.2 wt % DDM + POPC + DOTAP), below the 1:1 mass ratio of DDM:PR required for the hydrophobic membrane protein PR to remain soluble during synthesis.⁴⁸ The maximum loading of proteorhodopsin into these films is limited by its solubility in water, which may be increased by increasing the relative concentrations of the lipid surfactants (POPC and DOTAP). Careful tuning of composition and synthesis conditions for PR-containing silica-surfactant films with 62.5 DDM: 6.1 POPC: 1.4 DOTAP: 22.5 SiO₂: 7.5 npropyl-SiO_{1.5} by weight has enabled high PR loadings to be obtained, although with reduced extents of mesostructural order at higher PR contents. Further improvements in mesostructural ordering of the films with high protein loadings may require higher concentrations of structure-directing surfactants at the expense of lower silica contents or careful manipulation of external influences such as material-substrate interactions or directed nucleation sites.

Local Compositions and Interactions at Mesochannel Surfaces. At the atomic scale, complicated interactions between organosiloxanes, silica precursors, surfactants, and proteins govern the assembly of mesostructured silicasurfactant-protein composites. In particular, the interactions of the surfactant species at the mesostructured silica walls are expected to provide insights into the local compositional features that are key to balancing the combined proteinstability and structure-directing functions of the different surfactants. Conventional one-dimensional (1D) solid-state $^{1}\mbox{H}\mbox{, }^{13}\mbox{C}\mbox{, and }^{29}\mbox{Si NMR}$ analyses are sensitive to differences in local bonding environments, which can lead to differences in the isotropic chemical shifts of these NMR-active nuclei that enable different types of chemical species in a material to be identified. To establish the relative proximities or interactions of different moieties with each other, two-dimensional (2D) heteronuclear correlation (HETCOR) NMR techniques are used to correlate the isotropic chemical shifts of nearby (<1 nm) dipole-dipole-coupled nuclei. Such 2D HETCOR analyses provide detailed atomic-scale insights into the interactions of the coassembled surfactant and silica species, including at the mesochannel surfaces. For example, a 2D ²⁹Si{¹H} HETCOR NMR spectrum in Figure 5a of the same 5 wt % PR-containing film as previously discussed (Figures 3b and 4b) reveals correlated ²⁹Si and ¹H signal intensity that can be assigned to specific moieties that are within nanoscale proximities of one another. Five distinct ²⁹Si NMR signals are observed and can be assigned to ²⁹Si moieties in different

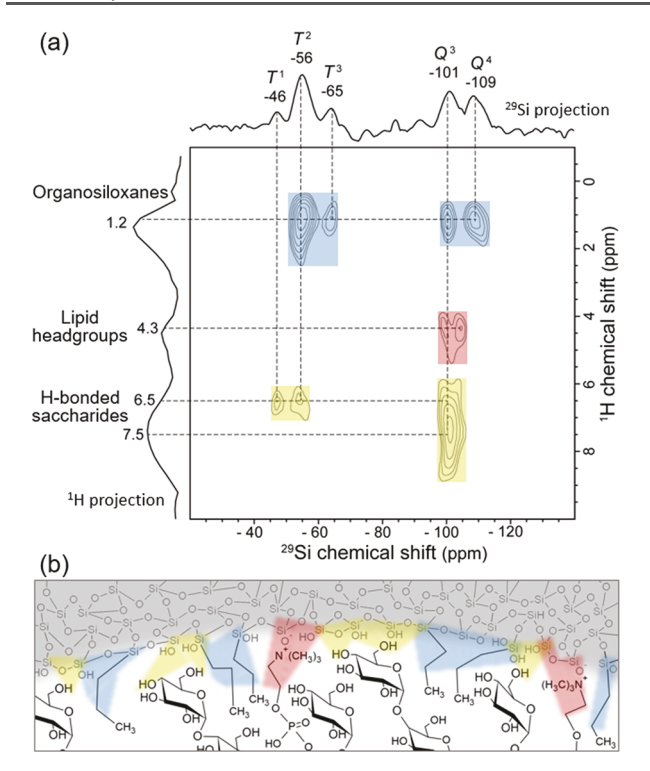


Figure 5. (a) Solid-state 2D ²⁹Si{¹H} HETCOR NMR spectrum for the same mesostructured 5 wt % PR, 59.4 wt % DDM, 5.8 wt % POPC, 1.3 wt % DOTAP, 21.4 wt % SiO₂, and 7.1 wt % *n*-propyl SiO_{1.5} film for which the SAXS patterns in Figures 3b and 4b were obtained. The spectrum was acquired at 298 K, 11.7 T, and 12.5 kHz MAS with a short 1.0 ms cross-polarization contact time used to probe strong ²⁹Si-¹H dipolar couplings between ²⁹Si and ¹H moieties in subnanoscale proximity. 1D projections of correlated ²⁹Si and ¹H intensities are shown on the horizontal and vertical axes, respectively. (b) Schematic diagram of molecular moieties at the mesochannel walls, which are consistent with the 2D NMR results. Proximate silicaorganosiloxane (blue) and silica—surfactant (red) interactions are highlighted.

bonding environments. Fully cross-linked four-coordinate 29 Si Q^4 silica species are assigned to the signal at -110 ppm, and partially cross-linked Q^3 silica species with a silanol group are assigned to the 29 Si NMR signal at -101 ppm. 49 Organosiloxane T^1 , T^2 , and T^{3} 29 Si moieties are associated with 29 Si NMR signals at -46, -56, and -65 ppm, respectively, where T^{3-n} represents a tetrahedrally coordinated 29 Si atom with one Si–C covalent bond, 3-n Si–O–Si linkages, and n silanol groups. 49 These 29 Si organosiloxane moieties originate from the hydrolysis of n-propyltriethoxysilane (PTEOS) silica precursor molecules and contribute to increased mesostructural order of the films.

Five distinct regions of correlated 29 Si and 1 H intensity are observed in the 2D 29 Si{ 1 H} HETCOR NMR spectrum of Figure 5a, which reveal distinct types of dipole–dipole-coupled silica moieties that are in nanoscale proximities to various organosiloxane, adsorbed water, and surfactant 1 H species. Specifically, the 1 H NMR signal at 1.2 ppm from alkyl moieties on the organosiloxanes and surfactants is correlated with 29 Si NMR intensity at -56, -65, -101, and -109 ppm associated with T^{2} , T^{3} , Q^{3} , and Q^{4} silica species, respectively, as highlighted in blue. The majority of the correlated signal intensities between the 1 H signal at 1.2 ppm and the 29 Si signals at -56 and -65 ppm from the T^{n} moieties is due to the

strong dipolar interactions that are associated with the covalently bonded organosiloxane propyl groups (Figure 5b). The ¹H signal at 4.3 ppm is attributed to the cationic lipid headgroups of the DOTAP and POPC, which is consistent with the solution-state 2D ¹³C-¹H NMR correlation spectra of these lipids (Figures S1 and S2) and literature reports⁵⁰ and which exhibits correlated intensity with the ²⁹Si signal centered at -101 ppm (red) from hydrophilic Q^3 silica moieties. Importantly, the ¹H signals in the region of 6.5-7.5 ppm manifest hydrogen-bonded moieties associated with the DDM surfactant species, which are strongly correlated with the ²⁹Si signal centered at -101 ppm (yellow) from partially crosslinked Q³ moieties and more weakly correlated with ²⁹Si signals at -46 and -56 ppm (yellow) from partially cross-linked T^1 and T^2 moieties, all of which have pendant silanol groups. These results provide evidence for the nanoscale proximity of the DDM species near the mesochannel walls and their role in directing the coassembly of the mesostructured silicasurfactant matrix. There are no correlated signals that would suggest strong direct interactions between the proteorhodopsin guests and the silica matrix, which is consistent with the conformational freedom of the protein discussed below. The 2D ²⁹Si{¹H} HETCOR NMR analyses thus establish strong interactions between the silica mesochannel surfaces and both the saccharide headgroups of the DDM surfactant species and the cationic headgroups of the DOTAP or POPC lipid species. The results corroborate the schematic diagrams in Figure 2b, which depict proteorhodopsin in the mesochannel centers of the PR-containing silica—surfactant films.

Effects of Non-Native Host Environments on Proteorhodopsin Photocycle Kinetics. Under native conditions, photoactivation of proteorhodopsin induces a series of cyclical conformational changes that transport H+ cations along its associated ion channel and across the cell membranes of marine bacteria. This photocycle is dependent, in particular, on the D97 residue of proteorhodopsin (Figure 1a), which is a key H⁺ acceptor that, if already protonated, discourages net H⁺ transport.⁵¹ The protonation state of the D97 residue and its pK_a (the pH value at which half of these residues are protonated) are therefore integral to the function of proteorhodopsin. Importantly, the pK_a of residue D97 of proteorhodopsin is significantly influenced by its local environment. For example, in similar DDM micellar solutions, the p K_{aD97} is 6.5 for wild-type oligomeric proteorhodopsin and 7.2 for the monomer-enriched E50Q mutant of proteorhodopsin. 25,52 Similarly, the coassembled surfactants and silica species in the mesostructured films influence the local chemical environments of the PR guest molecules, including the D97 residue and, importantly, the light-responsive retinal group. The latter can be probed by using UV-visible spectroscopy to measure the pH-dependent optical absorbance transition of the retinal group. Doing so reveals a p K_{aD97} of 6.2 for monomeric PR in the DDM + POPC + DOTAP-directed silica films, a value that is higher than previously reported (p K_{aD97} 5.6) for PR in POPC + DOTAP liposomes without DDM, 43 and significantly lower than the pK_{aD97} of 8.2 observed for PR in DDM + DHPC-directed silica films. The 2-unit lower p K_{aD97} value for PR in DDM + POPC + DOTAP-directed silica films results in a significantly larger percentage (86%) of H+transporting PR monomers with a deprotonated D97 residue compared to DDM + DHPC-silica films for which only 6% of the D97 residues are deprotonated at pH 7. These large differences in pK_{aD97} appear to arise from differences in ion

distributions near function-dependent residues along the PR ion channel, which are sensitively influenced by the compositions and architectures of the cationic and zwitterionic lipid components in mesostructured PR-silica-surfactant films with otherwise similar compositions.

The fact that the proteorhodopsin-stabilizing lipid components so strongly affect protonation of the interior D97 residue suggests extensive nonlocal conformational changes of the PR guests that are expected to influence their light-activated photocycle kinetics as well. Such effects can be probed by timeresolved UV-visible light spectroscopy, which measures the relative absorbance of light by PR molecules as they undergo photoactivated conformational changes during their photocycle. The retinal chromophore of PR (which absorbs green light, giving the protein its distinct purple-red color) is sensitive to changes in its local environment, which are manifested by differences in the wavelength of light that the retinal absorbs. As a consequence, the relative absorbance of light by the retinal is a function of both the wavelength of the incident light and time as the photocycle proceeds. Timeresolved UV-visible absorbance spectra of PR in different chemical environments can therefore be compared to elucidate the effects that different hosts or conditions have on the photocycle kinetics of PR. In particular, it is possible to monitor the photocycle of monomeric PR with time steps that are sufficiently short so that both the accumulation and depletion of photointermediates are observed. This is demonstrated in the time-resolved UV-visible light spectra in Figure 6 for 5 wt % PR-containing DDM + POPC + DOTAP-directed silica films at different pH conditions at wavelengths of 410, 500, 570, and 630 nm. For an assynthesized 5 wt % PR-silica-surfactant film at pH 4.1 (chosen to balance mesophase coassembly and PR stability considerations during synthesis, as discussed above), the low pH conditions result in less than 1% of the D97 residues of monomeric PR guests being deprotonated. Under these conditions, a distinct photocycle with three spectrally resolved intermediates (K, L, and N) and one spectrally silent intermediate (PR') are observed, as shown in Figure 6a.⁵¹

The UV-visible light spectra of PR in as-synthesized DDM + POPC + DOTAP-directed silica-surfactant films (Figure 6a) show no absorbance changes at 410 nm throughout the PR photocycle, which is characteristic of proteorhodopsin with a dominating fraction of protonated (i.e., inactive) D97.51 At early times following green laser excitation, mesostructured silica-surfactant films with PR show a positive difference absorbance intensity at 570 and 630 nm and a negative intensity at 500 nm. The intensities at each of these wavelengths decay monotonically toward zero at long times, similar to spectra observed for PR in DDM micellar solutions and in E. coli lipids under aqueous acidic conditions, which also show positive difference intensities at 570 and 630 nm and negative intensities for 500 nm immediately after light excitation.⁵¹ To evaluate these differences quantitatively, the spectra were fit by approximating the absorbance intensities at each wavelength as a sum of monoexponential decays with wavelength-specific pre-exponential factors and mutual (wavelength-nonspecific) time constants. These time constants are shared across the set of linear equations and represent the characteristic time scales for the serial light-activated interconversions of PR between two or more down-cycle photointermediates. For the spectra in Figure 6a, three exponentials corresponding to time constants $\tau_1 = 1$ ms, $\tau_2 =$

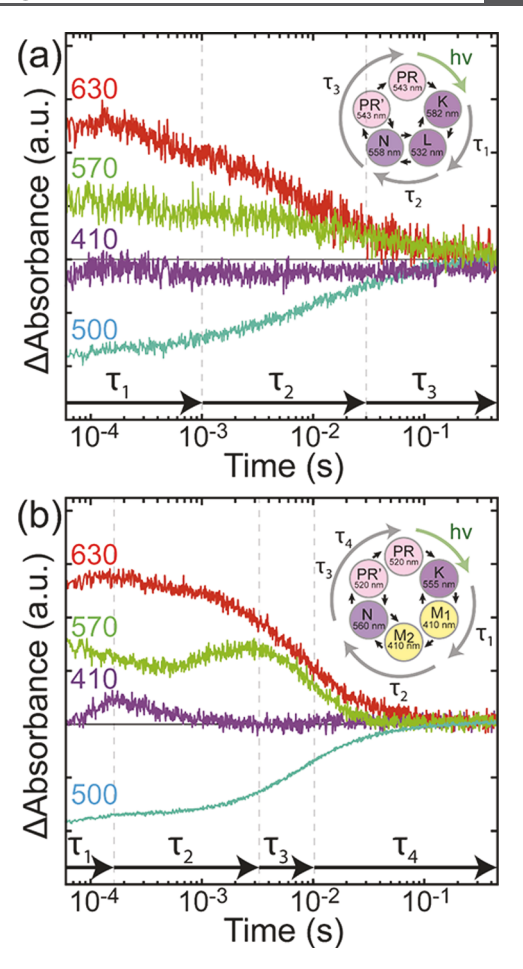


Figure 6. Time-resolved UV—visible light spectra showing transient absorbance traces at wavelengths of 410, 500, 570, and 630 nm for monomeric proteorhodopsin (PR) in PR-containing silica—surfactant films under varying pH conditions: (a) as-synthesized at pH 4.1 and (b) hydrated for 1 week at pH 9. Schematic diagrams are provided for the (a) acidic and (b) alkaline photocycles of proteorhodopsin.

19 ms, and τ_3 = 165 ms were used to produce accurate fits. By comparison with other photocycle analyses of PR in *E. coli* lipids, ⁵¹ these characteristic times (the reciprocals of which represent apparent rate coefficients) are associated with the rates of interconversion between specific PR photointermediates: τ_1 to the conformational change that occurs as the *K* conformer isomerizes into the *L* intermediate, τ_2 to the conversion of the *L* conformer into the *N* intermediate, and τ_3 to the rate-limiting conversions of the *N* conformer into the PR' intermediate and the subsequent isomerization of PR' back to the original PR conformation, whereupon the cycle can repeat. For the proteorhodopsin-containing mesostructured silica—surfactant films investigated here, acidic conditions are not suitable for selective H⁺ transport.

By comparison, moderately alkaline pH conditions lead to substantial deprotonation of the key D97 residue of proteorhodopsin in DDM + POPC + DOTAP-directed silica films, which is required for H⁺ transport. Previously, photoactivation of proteorhodopsin at pH 9.5 in membrane-fragments encased in polyacrylamide was shown to produce a spectrally distinct photocycle that transported a H⁺ cation through the PR ion channel. To observe this photocycle in 5 wt % PR-containing DDM + POPC + DOTAP-directed silica materials, the films were hydrated for 1 week in pH 9

buffer containing 50 mM K_2HPO_4 and 150 mM HCl. Importantly, due to the low pK_{aD97} value of 6.2 of this material, these conditions result in deprotonated D97 residues in 99.8% of PR monomers in the film. The effect of alkaline hydration on this film can be observed macroscopically as a displacement of the maximum absorbance of the retinal of PR to shorter wavelengths, causing the film to change from purple to red. The photocycle of proteorhodopsin under these pH conditions has been previously reported and involves conformational changes into six photocycle intermediates (PR, K, M_1 , M_2 , N, and PR', as shown in the inset of Figure 6b). S4

In fact, the complicated photocycle kinetics of PRcontaining silica-surfactant films at pH 9 resemble the light absorbance properties of native-like PR. Specifically, the accumulation and decay of the 410 nm trace, which is not observed for as-synthesized acidic PR-silica-surfactant films (Figure 6a), is attributable solely to the populations of the M intermediates and indicates that proteorhodopsin undergoes a native-like photocycle.⁵¹ Interestingly, this 410 nm trace rises to a maximum at \sim 500 μ s, significantly slower than monomeric PR in DDM micellar solutions, which peak at \sim 60 μ s for a similar alkaline pH value, ²⁹ and is instead more similar to the absorbance spectra observed for wild-type proteorhodopsin in POPC bicelles.⁵⁵ This is notable because the 5 wt % PR-silica-surfactant films analyzed in Figure 6 contain 59.4 wt % DDM and only 7.1 wt % POPC + DOTAP, suggesting that interactions between the protein, POPC, and DOTAP significantly impact the PR photocycle. While the accumulation and depletion of the M intermediate of PR, which maximally absorbs at 410 nm, can be observed on its own, the absorbance spectra of the PR, K, N, and PR' photointermediates overlap, absorbing maximally at approximately 520, 555, 560, and 520 nm, respectively.⁵⁴ The absorbance-difference data at 570 nm show initially positive intensity, which is attributable to the accumulation of the K intermediate conformer, and decays until \sim 300 μ s, at which point a second increase in intensity is observed, corresponding to an increase in the population of the N intermediate. These results correlate well with the accumulation and decay of the M intermediates, as characterized by the 410 nm spectral data, which are between the K and N intermediates in the PR photocycle. Although not directly attributable to the populations of specific photocycle intermediates, the absorbance-difference data at 500 and 630 nm show distinct decreases in intensity at ~3 ms, which are similar to the behavior of monomeric proteorhodopsin in DDM micelles at similar wavelengths.²⁹ Importantly, the similar UV-visible light spectral behavior of proteorhodopsin in alkaline-hydrated mesostructured silica-surfactant films, compared to PR in native-like micellar solutions and lipid bicelles, demonstrates that functionally active PR guest species can be obtained by rehydrating the films from pH 4.1 to alkaline conditions, such as pH 9.

Based on global fit analyses of transient UV-visible spectroscopy results in Figure 6b, four exponentials accurately described the photocycle kinetics of PR in DDM + POPC + DOTAP-directed silica materials under alkaline conditions at pH 9. Specifically, the absorbance-difference spectra lead to distinct time constants of $\tau_1 = 95 \ \mu s$, $\tau_2 = 2 \ ms$, $\tau_3 = 8 \ ms$, and $\tau_4 = 60 \ ms$. Following the analyses of Idso et al. for monomeric PR in DDM micellar solutions, $\tau_2 = \tau_3 = 0 \ ms$ attributed to the conversion of the $\tau_3 = 0 \ ms$ conformer into the $\tau_3 = 0 \ ms$ in termediate, $\tau_4 = 0 \ ms$ intermediate, $\tau_4 = 0 \ ms$ interme

associated with sequential conversions between the M_1 , M_2 , and N intermediates, and τ_3 and τ_4 correspond to serial conversions between the N, PR', and PR intermediates. Notably, the longest time constant (τ_4 = 60 ms) observed for monomeric PR in DDM + POPC + DOTAP-directed silica—surfactant films is significantly shorter than the corresponding time constant of 82 ms for PR in DDM micelles, as reported by Idso et al. ²⁹ Comparison of these analyses suggests that the time constants τ_3 and τ_4 correspond to the rate-limiting steps N to PR' and PR' to PR associated with H+ transport of PR in the mesostructured silica—surfactant host film, which are dependent on and can be mediated by interactions between PR molecules and the structure-directing and stabilizing DDM surfactant species and POPC and DOTAP lipids.

Mechanical and Thermal Stability Properties of Proteorhodopsin-Containing Silica Films. The composition-structure relationships of protein-host materials influence their mechanical properties. Specifically, the elastic moduli and hardnesses of mesostructured PR-containing silica—surfactant films are dependent on the extent of mesostructural ordering and PR loading of the films. This is evident in Figure 7, which shows nanoindentation analyses of PR-containing mesostructured silica—surfactant films as a function of proteorhodopsin content over the range 0–44 wt % PR. Previously, relatively poor mechanical properties (0.005 GPa mean hardness,

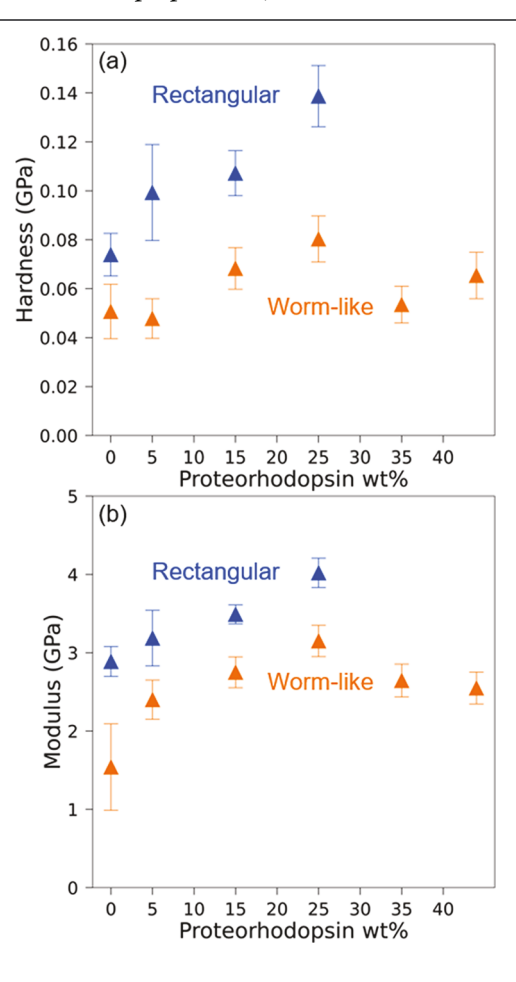


Figure 7. Nanoindentation analyses of the (a) hardness and (b) elastic moduli of mesostructured silica—DDM + POPC + DOTAP films with different monomeric proteorhodopsin loadings: 0, 5, 15, 25, 35, and 44 wt % PR with rectangular (blue) or wormlike (orange) mesostructural order.

0.260 GPa mean modulus) were reported for a 5 wt % PRcontaining silica-surfactant film with worm-like mesostructural order that was synthesized using DDM, 1,2-diheptanoylsn-glycero-3-phosphocholine (DHPC), and sodium perfluorooctanoate.5 Here, for comparison, 5 wt % PR-containing DDM + POPC + DOTAP-directed mesostructured silicasurfactant films with worm-like or rectangular mesostructural ordering were synthesized and their mechanical properties compared. The worm-like material exhibited a hardness of 0.05 \pm 0.01 GPa (Figure 7a) and modulus of 2.40 \pm 0.26 GPa (Figure 7b), while the rectangular mesostructured PR-silicasurfactant material was measured to have a hardness of 0.10 \pm 0.02 GPa (Figure 7a) and a modulus of 3.19 \pm 0.35 GPa (Figure 7b), values of which are at least an order of magnitude greater than previous PR-containing films. For PR-containing DDM + POPC + DOTAP-directed mesostructured silicasurfactant films over the range 0-25 wt % PR loading, rectangular mesostructural ordering exhibited on average a 0.04 GPa higher hardness and 0.94 GPa higher modulus, compared to similar films with wormlike mesostructural ordering. The increased hardnesses and moduli of PRcontaining silica-surfactant films with rectangular, compared to wormlike, mesostructural ordering is attributed in part to the periodic organization and thickness of silica walls between the mesochannels over which stresses are relatively evenly distributed.50

PR loading is also observed to have a significant effect on the mechanical properties of the mesostructured silica-surfactant films. For example, PR-containing films with wormlike mesostructural ordering exhibited hardnesses of 0.05 ± 0.01 GPa without PR and up to 0.08 ± 0.01 GPa for a 25 wt % PR film (Figure 7a), while compositionally similar films with rectangular mesostructural ordering (the same films as in Figures 4a-d) exhibited hardnesses of 0.07 \pm 0.01 GPa without PR and up to 0.14 ± 0.01 GPa for a 25 wt % PRcontaining film (Figure 7b). The moduli of the respective films similarly increased from 1.54 \pm 0.55 to 3.2 \pm 1.6 GPa for films with worm-like mesostructural order and from 2.9 \pm 0.19 to 4.0 ± 0.19 GPa for films with rectangular mesostructural order. Interestingly, the hardnesses and moduli of the films increased, even though the relative silica contents were lower in films with higher PR contents (with the ratios of all other species held constant). This is consistent with the relatively stiff properties of the seven aligned α -helices that constitute much of each PR monomer and is supported by recent investigations that have reported similar moduli and trends for other α -helix-containing proteins.⁵⁷ However, otherwise identical mesostructuredcontaining silica-surfactant films with higher PR loadings of 35 and 44 wt % PR and reduced extents of worm-like mesostructural order (Figure 4) exhibited less robust mechanical properties, with hardnesses of 0.05 ± 0.01 and 0.07 ± 0.01 GPa, and moduli of 2.64 ± 0.21 and 2.55 ± 0.2 GPa, respectively. These hardness and modulus values are significantly lower than those measured for the mesostructured 25 wt % PR films with similar worm-like mesostructural order. This is due in part to the lower silica contents of the 35 and 44 wt % PR-containing films (19.5 and 16.8 wt % silica, respectively), compared to the 25 wt % PR film (22.5 wt % silica), which provides the most robust host matrix for the film compositions and conditions examined. These results demonstrate that, for the compositions and conditions investigated, a high extent of mesostructural order and 25 wt % PR loading correlate with increased film hardness and modulus, observations that are supported by trends in other materials in which high-modulus guest molecules have been incorporated to increase the bulk modulus of composite materials. The moduli and hardnesses of rectangular PR-containing silica—surfactant films are significantly greater than previous formulations of similar materials and comparable with nonprotein-containing mesostructured silica materials. 31,59

Similarly, the thermal stability of proteorhodopsin guest molecules in silica—surfactant host matrices also depends on the compositions of the films and their extents of mesostructural order. Previously, DDM + DHPC + PFO-directed host films were shown to exhibit higher thermal stability of PR (up to approximately 97 °C) compared to PR in P123 triblock copolymer-directed films or PR in native-like phospholipid membranes.⁵ Figure 8 shows the results of

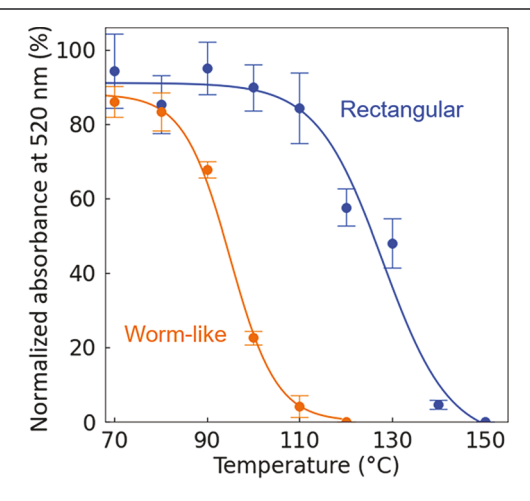


Figure 8. Normalized UV—visible light absorbance intensities at 520 nm for mesostructured 5 wt % PR, 59.4 wt % DDM, 5.8 wt % POPC, 1.3 wt % DOTAP, 21.4 wt % $\rm SiO_2$, and 7.1 wt % $\it n$ -propyl $\rm SiO_{1.5}$ films with rectangular (blue) and wormlike (orange) mesostructural ordering after heat treatment for 24 h. The absorbance at 520 nm was measured for the center of each sample following heat treatment and normalized against a similar measurement taken prior to heat treatment.

normalized static UV-visible light absorbance measurements, as functions of temperature, for 5 wt % PR incorporated into DDM + POPC + DOTAP-directed rectangular and worm-like mesostructured silica films. Interestingly, proteorhodopsin guest molecules exhibited significantly greater thermal stabilities, up to approximately 110 °C after 2 h in wellordered rectangular mesostructured silica-surfactant materials, compared to compositionally identical host matrices with worm-like structures. For PR in the rectangular mesostructured host, 85% normalized intensity at 520 nm was retained at 110 °C and 48% at 130 °C, which represents a significant increase in the thermal stability of PR, compared to other previously reported synthetic host materials.⁵ The retention of PR stability up to 110 $^{\circ}\text{C}$ and the gradual loss in absorbance at 520 nm (attributed to denaturation of PR) can be observed visually as a loss in the purple color of the film (Figure S7). Significant and essentially complete denaturation of the PR guest molecules, at 140 and 150 °C, respectively, can be observed visually as a transition to a yellow film, the color associated with denatured PR.

For comparison, heat treatment analyses were conducted on films with identical compositions but with wormlike

mesostructural order. As shown by the orange data points in Figure 8, PR guest molecules in films with wormlike structures exhibited significantly lower normalized absorbances at 520 nm following heat treatment over the range 70-120 °C. More specifically, PR in DDM + POPC + DOTAP-directed silica films with worm-like mesostructural order retained approximately 80% absorbance at 520 nm up to 80 °C, similar to PR in phospholipid membranes.⁵ However, PR in such films exhibited significantly diminished absorbance above 90 °C, temperatures at which PR in phospholipid bilayers is also fully denatured. The different thermal stabilities of PR in DDM + POPC + DOTAP-directed mesostructured silica films with rectangular versus wormlike mesostructural order are thought to be due, in part, to differences in the local hydration environments of hydrophilic moieties at the extracellular and cytoplasmic ends of PR.60,61 Such moieties are expected to be influenced by interactions with the structure-directing surfactant species that depend on the extent of mesostructural order. Hydrophilic protein loops can exchange protons with surrounding water molecules, and environment-induced changes in hydration have been shown to have significant effects on the photocycle kinetics of PR.62 The normalized absorbance data in Figure 8 suggest that lower extents of mesoscale order perturb the hydration of these hydrophilic moieties and their interactions with surrounding water molecules, resulting in unfavorable distributions of PR hydration that reduces their hydrothermal stability compared to similar host matrices with more ordered mesoscale structures.

CONCLUSIONS

Mesostructured silica-surfactant materials have emerged as promising hosts to harness the unique and diverse functionalities of transmembrane proteins in macroscopic material morphologies such as thin films. The mesostructured proteorhodopsin-containing silica-surfactant materials reported here are well-ordered and have high membrane protein contents that exhibit native-like photocycle kinetics in transparent mechanically and thermally robust films. Complementary multiscale characterization techniques provide detailed insights into the protein-stabilizing and structuredirecting roles of surfactant species that promote coassembly of membrane proteins into mesostructured silica-surfactant hosts, along with the effects of different abiotic environments on the photocycle kinetics of the proteorhodopsin guests. SAXS analyses establish the alkyl chain lengths that promote high extents of rectangular mesostructural order in DDM + POPC + DOTAP-structure-directed films. Furthermore, this technique elucidates the effects of guest PR loading (up to 44 wt %) on the mesostructural ordering of silica-surfactant host films. Solid-state NMR corroborates that hydrophilic saccharide surfactant and charged lipid headgroups associate with hydrophilic moieties of the silica mesochannel wall by hydrogen-bonding and electrostatic interactions, respectively. The results demonstrate the importance of film composition, particularly the types and relative fractions of nonionic, zwitterionic, and cationic surfactants that contribute toward significantly improved mesostructural ordering, protein loadings, and mechanical properties, when compared to polymer, gel, glass, or previously reported mesostructured silica proteinhost materials. Nanoindentation analyses quantify the bulk mechanical properties of the films and showed that the hardness and modulus of a silica-surfactant film increased

with PR loading or mesostructural order. Additionally, thermal testing analyses reveal improved stability for PR guest moieties within well-ordered host materials. Complementary pK_a measurements and time-resolved UV-visible absorption spectroscopy establish that the inclusion of zwitterionic POPC and cationic DOTAP lipids significantly lower the pK_a of a key function-dependent residue of PR, thereby increasing the active populations of PR. Global fit analyses of the time-resolved UV-visible light spectra quantify influences of local chemical environments on the photocycle of proteorhodopsin, revealing that the kinetics of the rate-limiting step in the photocycle of PR are dependent on and can be mediated by the host material composition and structure. Such insights enable the selective incorporation of monomeric proteorhodopsin molecules into mesostructured silica-surfactant materials, with the tertiary structure of the protein largely unperturbed during the coassembly process. The high protein loading, mechanical robustness, and thermal stability of these DDM + POPC + DOTAP-silica-surfactant proteorhodopsinhost films open opportunities for harnessing transmembrane proteins in non-native environments. The results provide improved understanding of the complicated interactions that mediate PR functionality in nonbiological environments and provide criteria and guidance for selecting and optimizing the compositions and conditions that enhance PR performance. Given the archetypical seven- α -helical structure of proteorhodopsin, the insights are expected to apply to other transmembrane membrane proteins and provide general guidance for synthesizing abiotic host materials for incorporating proteins with diverse functions.

ASSOCIATED CONTENT

Supporting Information

The Supporting Information is available free of charge at https://pubs.acs.org/doi/10.1021/acs.chemmater.3c01303.

Solution-state 2D ¹H-¹³C HSQC NMR spectra for structure-directing surfactants; time-resolved UV-visible spectra of monomeric proteorhodopsin (in as-synthesized films at pH 4.1 and in silica-surfactant films at pH 9) for all wavelengths measured and used in the global fit analyses; and SEM, TEM, and optical images of mesostructured silica-surfactant-proteorhodopsin materials (PDF)

AUTHOR INFORMATION

Corresponding Author

Bradley F. Chmelka — Department of Chemical Engineering, University of California, Santa Barbara, California 93106-5080, United States; orcid.org/0000-0002-4450-6949; Email: bradc@ucsb.edu

Authors

Maxwell W. Berkow – Department of Chemical Engineering, University of California, Santa Barbara, California 93106-5080, United States

Hosu Gwak – Department of Chemical Engineering, University of California, Santa Barbara, California 93106-5080, United States

Matthew N. Idso − Department of Chemical Engineering, University of California, Santa Barbara, California 93106-5080, United States; © orcid.org/0000-0001-5685-0870

- Michael B. Schmithorst Department of Chemical Engineering, University of California, Santa Barbara, California 93106-5080, United States; ocid.org/0000-0002-8795-5082
- Bailey E. Rhodes Department of Materials, University of California, Santa Barbara, California 93106-5050, United States
- Brad D. Price Department of Physics, University of California, Santa Barbara, California 93106-9530, United States; Occid.org/0000-0002-2674-4206
- Daniel S. Gianola Department of Materials, University of California, Santa Barbara, California 93106-5050, United States
- Songi Han Department of Chemical Engineering, University of California, Santa Barbara, California 93106-5080, United States; Department of Chemistry and Biochemistry, University of California, Santa Barbara, California 93106-9510, United States; orcid.org/0000-0001-6489-6246

Complete contact information is available at: https://pubs.acs.org/10.1021/acs.chemmater.3c01303

Notes

The authors declare no competing financial interest.

ACKNOWLEDGMENTS

We are pleased that this paper is being featured in special issue in honor of Dr. Clement Sanchez, whose leadership, creativity, and depth of knowledge have inspired progress across interdisciplinary fields of materials research. This work was supported by the Institute for Collaborative Biotechnologies through grant W911NF-19-2-0026 from the U.S. Army Research Office. Materials characterization analyses were conducted using the shared facilities of the Materials Research Science and Engineering Center (MRSEC) at UC Santa Barbara: NSF DMR-2308708. The UC Santa Barbara MRSEC is a member of the Materials Research Facilities Network (www.mrfn.org). B.E.R. gratefully acknowledges support by the U.S. Department of Defense (DoD) through the National Defense Science & Engineering Graduate (NDSEG) Fellowship Program. We thank Prof. G. Váró for helpful discussions and Prof. M. Sherwin and NSF MCB-2025860 for the support of time-resolved UV-visible light spectroscopy measurements.

ABBREVIATIONS

PR, monomer-enriched ESOQ proteorhodopsin mutant; DM, n-decyl- β ,D-maltoside; DDM, n-dodecyl- β ,D-maltoside; HDM, n-hexadecyl- β ,D-maltoside; POPC, 1-palmitoyl-2-oleoyl-glycero-3-phosphocholine; DOTAP, 1,2-dioleoyl-3-trimethylam-monium-propane; DHPC, 1,2-diheptanoyl-sn-glycero-3-phosphocholine; TEOS, tetraethoxysilane; PTEOS, n-propyltriethoxysilane; IPTG, isopropyl β ,D-1-thiogalactopyranoside; SAXS, Small angle X-ray scattering; NMR, Nuclear magnetic resonance spectroscopy; HETCOR, heteronuclear correlation; HSQC, heteronuclear single quantum coherence spectroscopy

REFERENCES

- (1) Béjà, O.; Spudich, E. N.; Spudich, J. L.; Leclerc, M.; DeLong, E. F. Proteorhodopsin Phototrophy in the Ocean. *Nature* **2001**, *411* (6839), 786–789.
- (2) Sabehi, G.; Massana, R.; Bielawski, J. P.; Rosenberg, M.; Delong, E. F.; Beja, O. Novel Proteorhodopsin Variants from the Mediterranean and Red Seas. *Environ. Microbiol.* **2003**, 5 (10), 842–849.

- (3) Béjà, O.; Aravind, L.; Koonin, E. V.; Suzuki, M. T.; Hadd, A.; Nguyen, L. P.; Jovanovich, S. B.; Gates, C. M.; Feldman, R. A.; Spudich, J. L.; Spudich, E. N.; DeLong, E. F. Bacterial Rhodopsin: Evidence for a New Type of Phototrophy in the Sea. *Science* **2000**, 289 (5486), 1902–1906.
- (4) Engqvist, M. K. M.; McIsaac, R. S.; Dollinger, P.; Flytzanis, N. C.; Abrams, M.; Schor, S.; Arnold, F. H. Directed Evolution of Gloeobacter Violaceus Rhodopsin Spectral Properties. *J. Mol. Biol.* **2015**, 427 (1), 205–220.
- (5) Jahnke, J. P.; Idso, M. N.; Hussain, S.; Junk, M. J. N.; Fisher, J. M.; Phan, D. D.; Han, S.; Chmelka, B. F. Functionally Active Membrane Proteins Incorporated in Mesostructured Silica Films. *J. Am. Chem. Soc.* **2018**, *140* (11), 3892–3906.
- (6) Kalantari, M.; Yu, M.; Yang, Y.; Strounina, E.; Gu, Z.; Huang, X.; Zhang, J.; Song, H.; Yu, C. Tailoring Mesoporous-Silica Nanoparticles for Robust Immobilization of Lipase and Biocatalysis. *Nano Res.* **2017**, *10* (2), 605–617.
- (7) Califano, V.; Costantini, A. Immobilization of Cellulolytic Enzymes in Mesostructured Silica Materials. *Catalysts* **2020**, *10* (6), 706
- (8) Gupta, R.; Chaudhury, N. K. Entrapment of Biomolecules in Sol-Gel Matrix for Applications in Biosensors: Problems and Future Prospects. *Biosens. Bioelectron.* **2007**, 22 (11), 2387–2399.
- (9) Blin, J. L.; Gérardin, C.; Carteret, C.; Rodehüser, L.; Selve, C.; Stébé, M. J. Direct One-Step Immobilization of Glucose Oxidase in Well-Ordered Mesostructured Silica Using a Nonionic Fluorinated Surfactant. *Chem. Mater.* **2005**, *17* (6), 1479–1486.
- (10) Nordlund, G.; Sing Ng, J. B.; Bergström, L.; Brzezinski, P. A Membrane-Reconstituted Multisubunit Functional Proton Pump on Mesoporous Silica Particles. *ACS Nano* **2009**, 3 (9), 2639–2646.
- (11) Janshoff, A.; Steinem, C. Transport across Artificial Membranes—an Analytical Perspective. *Anal. Bioanal. Chem.* **2006**, 385 (3), 433–451.
- (12) Petkova, V.; Benattar, J.-J.; Zoonens, M.; Zito, F.; Popot, J.-L.; Polidori, A.; Jasseron, S.; Pucci, B. Free-Standing Films of Fluorinated Surfactants as 2D Matrices for Organizing Detergent-Solubilized Membrane Proteins. *Langmuir* **2007**, 23 (8), 4303–4309.
- (13) Bogdanov, M.; Dowhan, W.; Vitrac, H. Lipids and Topological Rules Governing Membrane Protein Assembly. *Biochim. Biophys. Acta BBA Mol. Cell Res.* **2014**, *1843* (8), 1475–1488.
- (14) Liang, H.; Whited, G.; Nguyen, C.; Stucky, G. D. The Directed Cooperative Assembly of Proteorhodopsin into 2D and 3D Polarized Arrays. *Proc. Natl. Acad. Sci. U. S. A.* **2007**, *104* (20), 8212–8217.
- (15) Liang, H.; Whited, G.; Nguyen, C.; Okerlund, A.; Stucky, G. D. Inherently Tunable Electrostatic Assembly of Membrane Proteins. *Nano Lett.* **2008**, *8* (1), 333–339.
- (16) Hua, D.; Kuang, L.; Liang, H. Self-Directed Reconstitution of Proteorhodopsin with Amphiphilic Block Copolymers Induces the Formation of Hierarchically Ordered Proteopolymer Membrane Arrays. J. Am. Chem. Soc. 2011, 133 (8), 2354–2357.
- (17) Neyshtadt, S.; Jahnke, J. P.; Messinger, R. J.; Rawal, A.; Segal Peretz, T.; Huppert, D.; Chmelka, B. F.; Frey, G. L. Understanding and Controlling Organic—Inorganic Interfaces in Mesostructured Hybrid Photovoltaic Materials. *J. Am. Chem. Soc.* **2011**, *133* (26), 10119—10133.
- (18) Kirmayer, S.; Dovgolevsky, E.; Kalina, M.; Lakin, E.; Cadars, S.; Epping, J. D.; Fernández-Arteaga, A.; Rodríguez-Abreu, C.; Chmelka, B. F.; Frey, G. L. Syntheses of Mesostructured Silica Films Containing Conjugated Polymers from Tetrahydrofuran—Water Solutions. *Chem. Mater.* **2008**, *20* (11), 3745—3756.
- (19) Melosh, N. A.; Steinbeck, C. A.; Scott, B. J.; Hayward, R. C.; Davidson, P.; Stucky, G. D.; Chmelka, B. F. Mesostructured Silica/Block Copolymer Composites as Hosts for Optically Limiting Tetraphenylporphyrin Dye Molecules. *J. Phys. Chem. B* **2004**, *108* (32), 11909–11914.
- (20) Segal-Peretz, T.; Jahnke, J. P.; Berenson, A.; Neeman, L.; Oron, D.; Rossini, A. J.; Chmelka, B. F.; Frey, G. L. Understanding and Promoting Molecular Interactions and Charge Transfer in Dye-

- Mediated Hybrid Photovoltaic Materials. J. Phys. Chem. C 2014, 118 (44), 25374–25391.
- (21) Phan, H.; Jahnke, J. P.; Chmelka, B. F.; Nguyen, T.-Q. Structural and Optoelectronic Properties of Hybrid Bulk-Heterojunction Materials Based on Conjugated Small Molecules and Mesostructured TiO₂. Appl. Phys. Lett. **2014**, 104 (23), 233305.
- (22) Ramírez, M. G.; Jahnke, J. P.; Junk, M. J. N.; Villalvilla, J. M.; Boj, P. G.; Quintana, J. A.; Calzado, E. M.; Chmelka, B. F.; Díaz-García, M. A. Improved Amplified Spontaneous Emission of Dye-Doped Functionalized Mesostructured Silica Waveguide Films. *Adv. Opt. Mater.* **2015**, 3 (10), 1454–1461.
- (23) Steinbeck, C. A.; Ernst, M.; Meier, B. H.; Chmelka, B. F. Anisotropic Optical Properties and Structures of Block Copolymer/Silica Thin Films Containing Aligned Porphyrin *J*-Aggregates. *J. Phys. Chem. C* **2008**, *112* (7), 2565–2573.
- (24) Granja, L. P.; Martínez, E. D.; Troiani, H.; Sanchez, C.; Soler Illia, G. J. A. A. Magnetic Gold Confined in Ordered Mesoporous Titania Thin Films: A Noble Approach for Magnetic Devices. *ACS Appl. Mater. Interfaces* **2017**, *9* (1), 965–971.
- (25) Han, C.-T.; Nguyen, K. D. Q.; Berkow, M. W.; Hussain, S.; Kiani, A.; Kinnebrew, M.; Idso, M. N.; Baxter, N.; Chang, E.; Aye, E.; Winslow, E.; Rahman, M.; Seppälä, S.; O'Malley, M. A.; Chmelka, B. F.; Mertz, B.; Han, S. Lipid Membrane Mimetics and Oligomerization Tune Functional Properties of Proteorhodopsin. *Biophys. J.* **2023**, *122* (1), 168–179.
- (26) Ernst, R. R.; Bodenhausen, G.; Wokaun, A. Principles of Nuclear Magnetic Resonance in One and Two Dimensions; The International series of monographs on chemistry; Clarendon Press; Oxford University Press: New York, NY, 1987.
- (27) Elena, B.; De Paëpe, G.; Emsley, L. Direct Spectral Optimisation of Proton—Proton Homonuclear Dipolar Decoupling in Solid-State NMR. *Chem. Phys. Lett.* **2004**, 398 (4–6), 532–538.
- (28) Fung, B. M.; Khitrin, A. K.; Ermolaev, K. An Improved Broadband Decoupling Sequence for Liquid Crystals and Solids. *J. Magn. Reson.* **2000**, *142* (1), 97–101.
- (29) Idso, M. N.; Baxter, N. R.; Narayanan, S.; Chang, E.; Fisher, J.; Chmelka, B. F.; Han, S. Proteorhodopsin Function Is Primarily Mediated by Oligomerization in Different Micellar Surfactant Solutions. J. Phys. Chem. B 2019, 123 (19), 4180–4192.
- (30) Oliver, W. C.; Pharr, G. M. An Improved Technique for Determining Hardness and Elastic Modulus Using Load and Displacement Sensing Indentation Experiments. *J. Mater. Res.* **1992**, 7 (6), 1564–1583.
- (31) Chemin, N.; Klotz, M.; Rouessac, V.; Ayral, A.; Barthel, E. Mechanical Properties of Mesoporous Silica Thin Films: Effect of the Surfactant Removal Processes. *Thin Solid Films* **2006**, 495 (1–2), 210–213
- (32) Gross, A. F.; Ruiz, E. J.; Tolbert, S. H. Effect of Framework Polymerization on the Phase Stability of Periodic Silica/Surfactant Nanostructured Composites. *J. Phys. Chem. B* **2000**, *104* (23), 5448–5461
- (33) Zhao, D.; Feng, J.; Huo, Q.; Melosh, N.; Fredrickson, G. H.; Chmelka, B. F.; Stucky, G. D. Triblock Copolymer Syntheses of Mesoporous Silica with Periodic 50 to 300 Angstrom Pores. *Science* **1998**, *279* (5350), 548–552.
- (34) Partha, R.; Krebs, R.; Caterino, T. L.; Braiman, M. S. Weakened Coupling of Conserved Arginine to the Proteorhodopsin Chromophore and Its Counterion Implies Structural Differences from Bacteriorhodopsin. *Biochim. Biophys. Acta BBA Bioenerg.* **2005**, 1708 (1), 6–12.
- (35) Albarracín, V. H.; Kraiselburd, I.; Bamann, C.; Wood, P. G.; Bamberg, E.; Farias, M. E.; Gärtner, W. Functional Green-Tuned Proteorhodopsin from Modern Stromatolites. *PLoS One* **2016**, *11* (5), No. e0154962.
- (36) Brinker, C. J.; Sehgal, R.; Hietala, S. L.; Deshpande, R.; Smith, D. M.; Loy, D.; Ashley, C. S. Sol-Gel Strategies for Controlled Porosity Inorganic Materials. *J. Membr. Sci.* **1994**, *94* (1), 85–102.
- (37) Guillemin, Y.; Etienne, M.; Aubert, E.; Walcarius, A. Electrogeneration of Highly Methylated Mesoporous Silica Thin

- Films with Vertically-Aligned Mesochannels and Electrochemical Monitoring of Mass Transport Issues. *J. Mater. Chem.* **2010**, *20* (32), 6799
- (38) Despas, C.; Vodolazkaya, N. A.; Ghanbaja, J.; Walcarius, A. Preparation of Ordered and Oriented Mesoporous Silica Thin Films Bearing Octyl or Hexadecyl Groups by Electrochemically Assisted Self-Assembly and Evaluation of Their Transport Properties. *J. Solid State Electrochem.* **2015**, 19 (7), 2075–2085.
- (39) ALOthman, Z. A Review: Fundamental Aspects of Silicate Mesoporous Materials. *Materials* **2012**, 5 (12), 2874–2902, DOI: 10.3390/ma5122874.
- (40) Otzen, D. Protein-Surfactant Interactions: A Tale of Many States. *Biochim. Biophys. Acta BBA Proteins Proteomics* **2011**, 1814 (5), 562-591.
- (41) Wu, S.-H.; Mou, C.-Y.; Lin, H.-P. Synthesis of Mesoporous Silica Nanoparticles. *Chem. Soc. Rev.* **2013**, 42 (9), 3862.
- (42) Štangar, U. L.; Hüsing, N. Alkyl-Glycoside Surfactants in the Synthesis of Mesoporous Silica Films. *Silicon Chem.* **2003**, 2 (3/4), 157–165.
- (43) Han, C.-T.; Song, J.; Chan, T.; Pruett, C.; Han, S. Electrostatic Environment of Proteorhodopsin Affects the PKa of Its Buried Primary Proton Acceptor. *Biophys. J.* **2020**, *118* (8), 1838–1849.
- (44) Lu, Y.; Fan, H.; Doke, N.; Loy, D. A.; Assink, R. A.; LaVan, D. A.; Brinker, C. J. Evaporation-Induced Self-Assembly of Hybrid Bridged Silsesquioxane Film and Particulate Mesophases with Integral Organic Functionality. *J. Am. Chem. Soc.* **2000**, 122 (22), 5258–5261.
- (45) Alberius, P. C. A.; Frindell, K. L.; Hayward, R. C.; Kramer, E. J.; Stucky, G. D.; Chmelka, B. F. General Predictive Syntheses of Cubic, Hexagonal, and Lamellar Silica and Titania Mesostructured Thin Films. *Chem. Mater.* **2002**, *14* (8), 3284–3294.
- (46) Nilsson, F.; Söderman, O.; Johansson, I. Physical—Chemical Properties of the n -Octyl β D -Glucoside/Water System. A Phase Diagram, Self-Diffusion NMR, and SAXS Study. *Langmuir* **1996**, *12* (4), 902–908.
- (47) Auvray, X.; Petipas, C.; Anthore, R.; Ricolattes, I.; Lattes, A. X-Ray-Diffraction Study of the Ordered Lyotropic Phases Formed by Sugar-Based Surfactants. *Langmuir* **1995**, *11*, 433–439.
- (48) Idso, M. N. Understanding and Optimizing the Interactions of Functional Species in Mesostructured Materials with Diverse Transport Properties. Ph.D. Thesis, University of California: Santa Barbara, 2017.
- (49) Lesaint, C.; Lebeau, B.; Marichal, C.; Patarin, J. Synthesis of Mesoporous Silica Materials Functionalized with N-Propyl Groups. *Microporous Mesoporous Mater.* **2005**, 83 (1–3), 76–84.
- (50) Cruciani, O.; Mannina, L.; Sobolev, A.; Cametti, C.; Segre, A. An Improved NMR Study of Liposomes Using 1-Palmitoyl-2-Oleoyl-Sn-Glycero-3-Phospatidylcholine as Model. *Molecules* **2006**, *11* (5), 334–344
- (51) Lakatos, M.; Lanyi, J. K.; Szakács, J.; Váró, G. The Photochemical Reaction Cycle of Proteorhodopsin at Low PH. *Biophys. J.* **2003**, 84 (5), 3252–3256.
- (52) Hussain, S.; Kinnebrew, M.; Schonenbach, N. S.; Aye, E.; Han, S. Functional Consequences of the Oligomeric Assembly of Proteorhodopsin. *J. Mol. Biol.* **2015**, 427 (6), 1278–1290.
- (53) Dioumaev, A. K.; Wang, J. M.; Bálint, Z.; Váró, G.; Lanyi, J. K. Proton Transport by Proteorhodopsin Requires That the Retinal Schiff Base Counterion Asp-97 Be Anionic. *Biochemistry* **2003**, 42 (21), 6582–6587.
- (54) Váró, G.; Brown, L. S.; Lakatos, M.; Lanyi, J. K. Characterization of the Photochemical Reaction Cycle of Proteorhodopsin. *Biophys. J.* **2003**, 84 (2), 1202–1207.
- (55) Lindholm, L.; Ariöz, C.; Jawurek, M.; Liebau, J.; Mäler, L.; Wieslander, Å.; Von Ballmoos, C.; Barth, A. Effect of Lipid Bilayer Properties on the Photocycle of Green Proteorhodopsin. *Biochim. Biophys. Acta BBA Bioenerg.* **2015**, *1847* (8), 698–708.
- (56) Miyoshi, H.; Matsuo, H.; Oku, Y.; Tanaka, H.; Yamada, K.; Mikami, N.; Takada, S.; Hata, N.; Kikkawa, T. Theoretical Analysis of Elastic Modulus and Dielectric Constant for Low- *k* Two-Dimensional Periodic Porous Silica Films. *Jpn. J. Appl. Phys.* **2004**, *43* (2), 498–503.

- (57) Perticaroli, S.; Nickels, J. D.; Ehlers, G.; O'Neill, H.; Zhang, Q.; Sokolov, A. P. Secondary Structure and Rigidity in Model Proteins. *Soft Matter* **2013**, *9* (40), 9548.
- (58) Reynaud, E.; Jouen, T.; Gauthier, C.; Vigier, G.; Varlet, J. Nanofillers in Polymeric Matrix: A Study on Silica Reinforced PA6. *Polymer* **2001**, 42 (21), 8759–8768.
- (59) Williford, R. E.; Li, X. S.; Addleman, R. S.; Fryxell, G. E.; Baskaran, S.; Birnbaum, J. C.; Coyle, C.; Zemanian, T. S.; Wang, C.; Courtney, A. R. Mechanical Stability of Templated Mesoporous Silica Thin Films. *Microporous Mesoporous Mater.* **2005**, 85 (3), 260–266.
- (60) Feng, J.; Mertz, B. Proteorhodopsin Activation Is Modulated by Dynamic Changes in Internal Hydration. *Biochemistry* **2015**, *54* (48), 7132–7141.
- (61) Hirschi, S.; Kalbermatter, D.; Ucurum, Z.; Lemmin, T.; Fotiadis, D. Cryo-EM Structure and Dynamics of the Green-Light Absorbing Proteorhodopsin. *Nat. Commun.* **2021**, *12* (1), 4107.
- (62) Hussain, S.; Franck, J. M.; Han, S. Transmembrane Protein Activation Refined by Site-Specific Hydration Dynamics. *Angew. Chem., Int. Ed.* **2013**, 52 (7), 1953–1958.